# Effect of vibration amplitude on mechanical response in machining of NiCrFe alloy

**Dinh-Quan Doan*, Huu-Chuyen Vu**

Faculty of Mechanical Engineering, Hung Yen University of Technology and Education

*Email: dinhquandoan@gmail.com

## Abstract

*This study investigates the cutting behavior of NiCrFe alloys under conventional and vibration-assisted cutting processes through molecular dynamics simulations. The study focuses on investigating the changes caused by tool vibrations on the mechanical response, deformation characteristics, and structural evolution during cutting at the nanoscale. The presence of vibration alters the interaction between the tool and the workpiece, creating periodic changes in contact and affecting the direction of mechanical load application. Simulations show that vibration not only reduces the cutting force but also influences the distribution and accumulation of shear strain around the cutting zone. Different vibration amplitudes are tested to clarify their role in mechanical deformation and material removal. The results show that increasing amplitude leads to a decrease in cutting force, a decrease in the friction coefficient, and an increase in the amount of material removed. These findings provide detailed atomic-level insights into enhanced material removal and morphological changes of machined surfaces under the influence of vibration.*

**Keywords:** Amplitude vibration, molecular dynamics simulation, NiCrFe alloy, vibration-assisted cutting.

## 1. Introduction

Nickel-based alloys such as Ni-Cr-Fe alloys are widely used in transportation, energy, and aerospace technologies due to their high strength, thermal stability, and strong resistance to oxidation and corrosion [1, 2]. These properties make them ideal for parts working in harsh environments, but Ni-based alloys are also classified as difficult-to-machine materials [3, 4]. NiFeCr alloys exhibit high mechanical performance and stable microstructure, but their high hardness and work-hardening tendency lead to strong cutting forces, high heat generation, and rapid tool wear during conventional machining [5]. These limitations reduce machining efficiency, especially since subsurface damage and residual stress play a significant role in the service life of machine parts. To overcome these challenges, many advanced machining

techniques have been studied, including electrochemical machining, laser machining, and abrasive waterjet machining [6, 7]. Among them, vibration-assisted cutting (VAC) has shown significant potential in improving the machining of hard and brittle materials [8, 9]. By creating controlled vibrations that impact the tool or workpiece, VAC can intermittently reduce tool and material contact, leading to reduced cutting forces, improved workpiece formation, and increased material removal rates. Previous studies on vibration-assisted machining have reported reduced cutting forces, friction coefficients, surface damage, and improved cutting stability compared to conventional machining [10, 11]. These improvements are particularly important for alloys with complex deformation behaviors, such as Ni-based systems and high-entropy alloys [12]. However, the fundamental mechanisms governing the mechanical properties, deformation mechanisms, and microstructure evolution during the VAC process of NiCrFe alloys are still not well understood. Experimental observation of interactions at the micro or nanoscale level is difficult due to technological limitations, high costs, and the transient nature of machining processes. Therefore, molecular dynamics (MD) simulation has emerged as a powerful tool for exploring cutting processes at the atomic level [13]. MD allows detailed analysis of stress-strain distribution and microstructure evolution, providing additional insights to experimental findings and supporting optimization of machining parameters [14].

Therefore, the present study investigates VAC of NiCrFe alloys using MD simulations. The effects of vibration amplitude on cutting forces, friction coefficient, shear strain distribution, microstructural evolution, and surface morphology are compared with conventional cutting (CC) methods. The study results aim to clarify the deformation mechanism of NiCrFe alloys under the influence of vibration and provide a theoretical basis for improving their machinability in practical applications.

### 1.2. Physical model and simulation setup

Figure 1 illustrates a simulation model of the NiCrFe alloy cutting process. This model features a spherical diamond cutting tool and a substrate made of NiCrFe alloy. The workpiece is modeled as a single crystal NiCrFe alloy with a face-centered cubic FCC structure. The model has dimensions of 250 Å × 150 Å × 120 Å, containing atoms with the alloy composition 51% Ni, 32% Fe, and 17% Cr. The workpiece is divided into three functional regions: a fixed layer to constrain rigid body motion, a thermostat layer to control temperature, and a Newtonian layer where atoms moved freely according to classical

Newtonian dynamics [15]. A diamond tool with a spherical geometry is used as the cutting tip and treated as a rigid body.

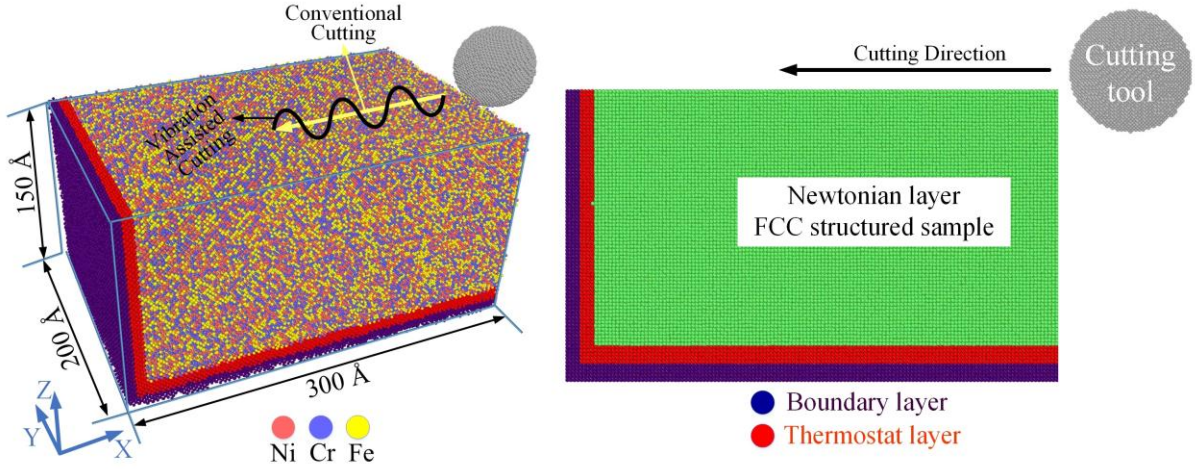


***Figure 1.*** Physical model for MD simulation of the cutting process of single-crystal NiCrFe alloy: the simulation model of the cutting process includes the substrate and the cutting tool.

The interactions between atoms in the NiCrFe alloy are described by the Embedded Atom Method (EAM) potential, which is widely used in other studies of metals and alloys [16]. Meanwhile, the interaction between the diamond tool and the metal atoms is modeled using the Lennard-Jones potential [17]. Before machining, the entire model undergoes energy minimization and thermal relaxation at 300 K using the NVT ensemble to achieve equilibrium. During cutting, the Newtonian atoms are integrated under the NVE ensemble to capture thermal variations induced by tool and workpiece interaction. A time step of 1 fs is used in the MD simulation. Periodic boundary conditions are applied along the Y-direction to minimize size effects, while the X- and Z-directions are treated as non-periodic. Both CC and VAC processes are simulated with similar machining parameters. The tool moves along the X-axis with a cutting speed of 100 m/s, a penetration depth of 20 Å, and a machining length of approximately 120 Å. In VAC mode, the tool moves along a sinusoidal trajectory determined by the vibration amplitude and frequency. A set of amplitudes ($A$ = 5-20 Å) and a fixed frequency of 15 GHz are chosen to study the influence of tool vibration on the mechanical behavior and material removal. These values are consistent with the frequencies commonly used in MD studies of vibration machining.

All molecular dynamics (MD) simulations to perform machining behavior testing of NiCrFe alloys under CC and VAC conditions are performed using LAMMPS software [18].

After the simulation, the results are analyzed in terms of structural evolution, strain distribution, and defect formation using OVITO [19].

## 3. Results and discussion

### *3.1. Mechanical properties of conventional cutting (CC) and vibration-assisted cutting (VAC)*

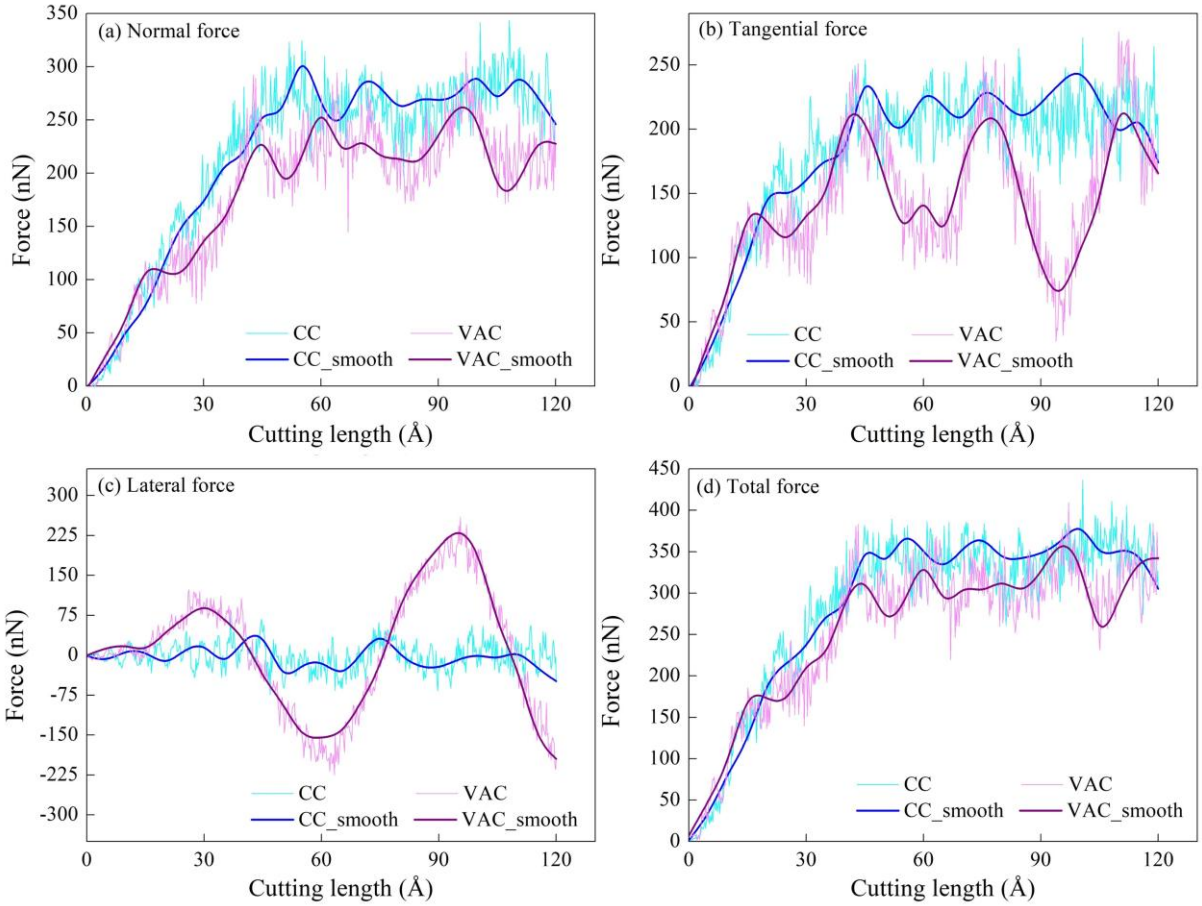


***Figure 2.*** Comparison of force components during conventional cutting (CC) and vibration-assisted cutting (VAC).

Figure 2 shows the cutting-force components change during machining under two conditions: without vibration and with vibration assistance. In the VAC simulation, the cutting tool is driven with an oscillation amplitude of 15 Å and a frequency of 15 GHz, creating a periodic contact cycle. Normal, tangential, lateral, and total forces are recorded at each cutting step to track the force development along the machining length. In Figure 2, the force components are displayed using two types of curves to highlight the difference between the raw and processed signals. The cyan curve for the non-vibration case and the light magenta curve for the VAC show the raw force data directly from the molecular dynamics

simulation, which contains strong fluctuations. The blue curve for the non-vibration case and the purple curve for the VAC show the smoothed data, in which small local fluctuations have been filtered out to make it easier to observe the force trend. This visualization helps to compare the force development under the two machining conditions. In terms of mechanical property, the initial stage of the cutting process (from 0 to about 15 Å) shows a nearly linear increase in force for both methods, indicating that the material undergoes mainly elastic deformation. When the cutting distance is larger than 15 Å, the force increases more strongly and becomes nonlinear, marking the beginning of plastic deformation and lattice displacement. As the tool moves deeper, from about 50 Å onwards, the process reaches a quasi-steady cutting stage. The force response of the two methods is clearly different. In the non-vibration, the forces only fluctuate slightly around a nearly constant value, while the forces show clear periodic oscillations with larger amplitudes due to the repeated contact and separation of the tool in the vibration-supported. The tangential and normal forces in the vibration-supported case also oscillate at twice the frequency of the transverse force, reflecting two collision events per vibration cycle in the longitudinal direction.

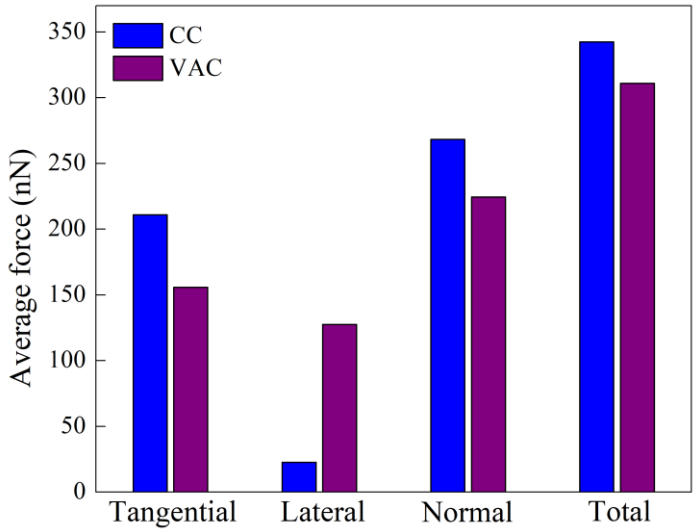


***Figure 3.*** Average force during conventional cutting (CC) compared to vibration-assisted cutting (VAC).

To compare the force differences more clearly, the force components in the steady stage from 50 Å to 120 Å are averaged, and the results are shown in Figure 3. The averaged tangential and normal forces in the CC process are noticeably higher than those in the VAC, while the average absolute value of the lateral force is larger in the VAC because it oscillates around zero. The average total force in VAC is much lower than in the non-vibration case, showing that applying vibration helps reduce the mechanical load on the cutting tool. It

should be noted that the shear force obtained in this study is higher than the values reported for HEA materials by both conventional and vibration-assisted cutting methods, reflecting differences in material composition and mechanical response [12]. These observations clearly indicate that the intermittent contact caused by vibration not only reduces the actual tool and workpiece contact time but also lowers the average cutting forces, even if the instantaneous peak forces may be higher at certain moments.

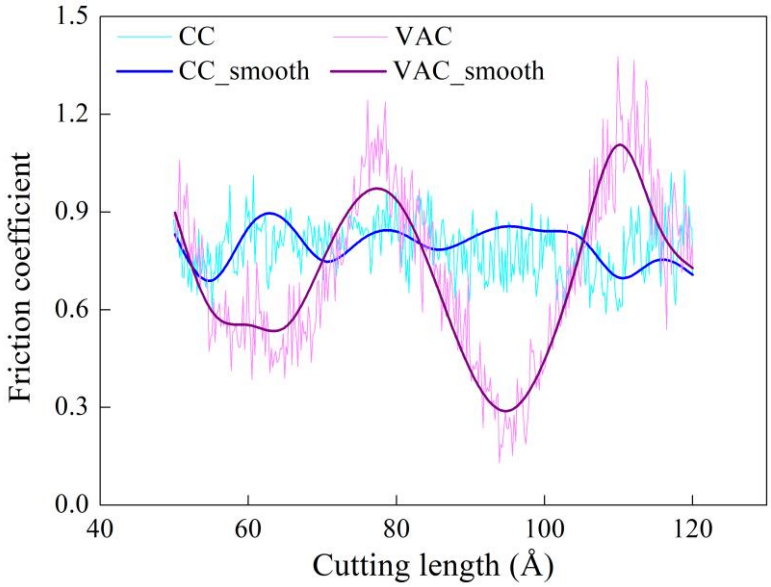


***Figure 4.*** Comparison of the change in friction coefficient during conventional cutting (CC) versus vibration-assisted cutting (VAC).

Figure 4 compares the change in friction coefficient during the CC and VAC processes. The coefficient of friction is defined as the ratio between the tangential and normal forces. The result shows that both cutting processes exhibit a gradual decrease in friction after the tool begins to stabilize on the workpiece, marking a transition from initial elastic deformation to a more stable cutting state. A notable difference emerges in the oscillation behavior of the two machining conditions. The VAC process displays a significantly larger oscillation amplitude than the CC process, resulting from periodic contact loss cycles caused by vibrations. After the process reaches a steady state, the smoothed curves show a clear difference in the average friction level. Specifically, the average friction coefficient in CC process is approximately 0.79, while VAC process with an oscillation amplitude of 15 Å yielded a lower average value, approximately 0.71. This reduction is closely related to the intermittent contact mechanism, meaning that as the tool moves along a sinusoidal trajectory in the XY plane, brief moments occur when the tool separates from the workpiece surface, significantly reducing the average contact area over time. Furthermore, the continuous

changes in sliding velocity and direction inherent in pulsating cutting cause the contact interface to alternate between sliding, separation, and impact. These rapid transitions inhibit the development of a stable adhesive contact, redistribute local stresses, and limit the accumulation of plastic deformation. Therefore, although the coefficient of friction in pulsating cutting fluctuates more strongly, its average value is still significantly lower than that of CC.

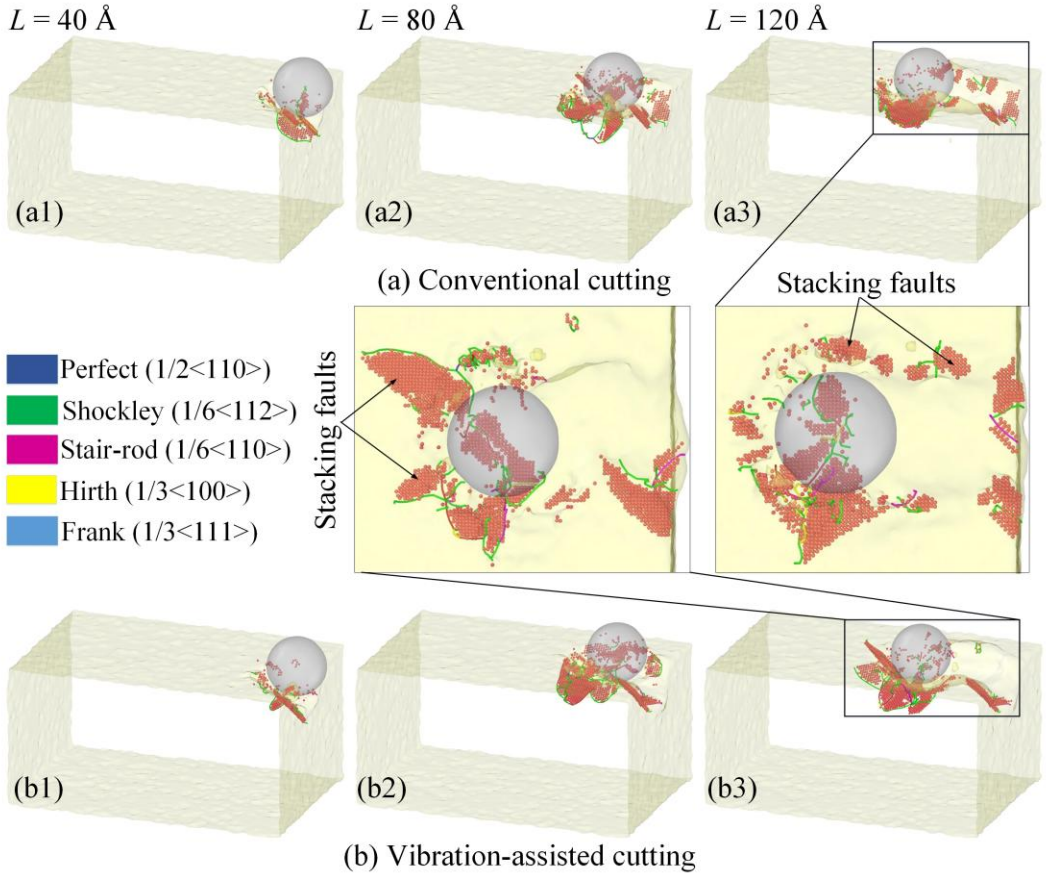


***Figure 5.*** Dislocation evolution (b1-b4 and d1-d4) in samples under conventional cutting (CC) and vibration-assisted cutting (VAC).

Figure 5 shows the evolution of dislocations in the samples as the cutting length increases under CC and VAC. DXA (Dislocation Extraction Algorithm) analysis reveals that cutting generates a highly deformed zone around the tool tip. At the early stage ($L$ = 40 Å), Shockley partial dislocations nucleate at the contact region, indicating slip on the {111} planes as the main deformation mechanism in the FCC structure. When the cutting length reaches 80 Å and 120 Å, the density of dislocations and defects such as stacking faults, Shockley and stair-rod dislocations increases, reflecting the accumulation of plastic deformation and the release of stored elastic energy. The two machining methods show

different dislocation behavior. In the CC process, the dislocations form a dense, interconnected network extending deep into the subsurface layer, and local Shockley dislocations develop into wide stacking-fault bands. In the VAC process, periodic vibrations interrupt the formation and development of dislocations, reducing their density and average length. The dislocations become more dispersed and their penetration depth is limited. The amorphous layer on the surface is also smaller, indicating better local structural resilience under the influence of vibrations. Figure 6 presents the total dislocation length according to the cutting distance during the CC and VAC. Both methods show a strong increase due to growing plastic deformation, but CC consistently produces longer dislocation lengths. At $L <$ 40 Å, dislocation formation in VAC is slower because vibration weakens early nucleation. Between 60-100 Å, both curves rise rapidly, though the increase is steeper in the CC, suggesting more severe deformation. At the final stage ($L \approx 120$ Å), the curves converge as the dislocation network approaches saturation. Nevertheless, VAC maintains a lower and more stable dislocation length, consistent with the more dispersed dislocation distribution observed in Figure 6.

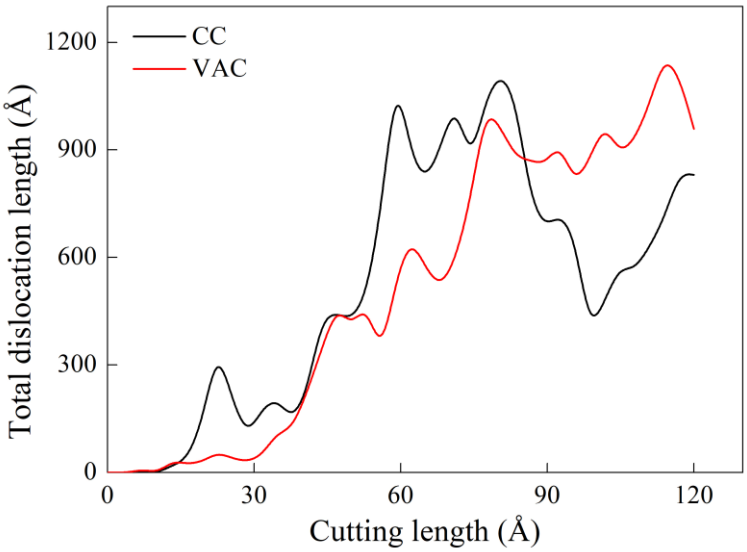


***Figure 6.*** Comparison of total dislocation length in the substrate during conventional cutting (CC) and vibration-assisted cutting (VAC).

*3.2. Effect of vibration amplitude*

Figure 7 illustrates the variation of cutting force components under different vibration amplitudes during machining at a vibration frequency of 15 GHz. The cutting process is performed at a vibration frequency of 15 GHz and a cutting speed of 100 m/s. At the initial stage ($L <$ 50 Å), the normal and tangential forces increase rapidly as the cutting tool begins

to contact the workpiece and causes local plastic deformation. As the cutting length increases to 50-120 Å, the force fluctuates around more stable average values. Increasing the vibration amplitude leads to a larger range of oscillation of the force components, clearly reflecting the effect of harmonic motion on the contact area. The normal and tangential forces vary cyclically with the oscillation period. Meanwhile, the transverse force oscillates around a value close to zero and increases in amplitude at higher oscillation amplitudes, indicating enhanced transverse shear strain and easier atomic movement toward both sides of the groove. The total force also exhibits harmonic oscillation, with the amplitude increasing proportionally with the oscillation amplitude, demonstrating stable energy transfer from the cutting tool to the workpiece.

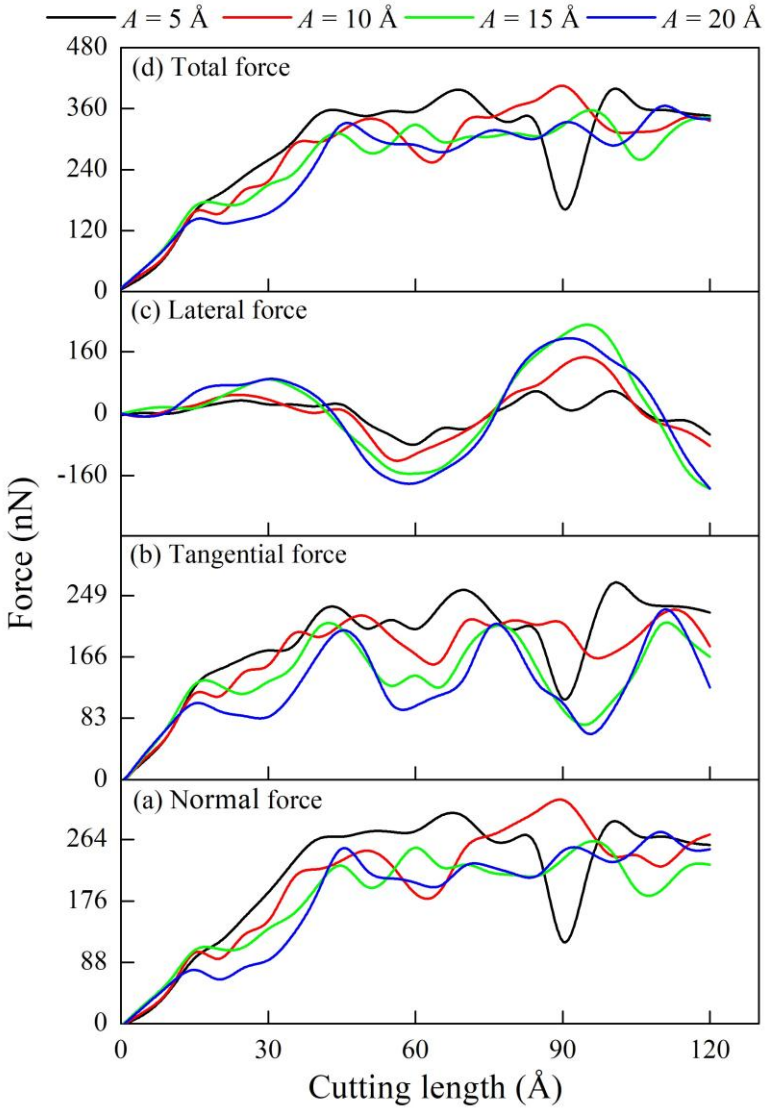


***Figure 7.*** Dependence of cutting force components on different vibration amplitudes.

Figure 8 shows the average cutting force versus vibration amplitude, calculated in the stable cutting zone from 50 to 120 Å. The result shows a significant effect of vibration amplitude on cutting force. Tangential and normal forces decrease with increasing amplitude, as vibration reduces the effective contact time between the tool and the workpiece surface. Conversely, lateral force increases with amplitude, reflecting increased lateral displacement and strain dispersion in the groove. Total force decreases slightly with increasing amplitude from 5 Å to 15 Å and remains almost constant at higher amplitudes, indicating that larger vibration amplitude reduces cutting force and improves material removal efficiency.

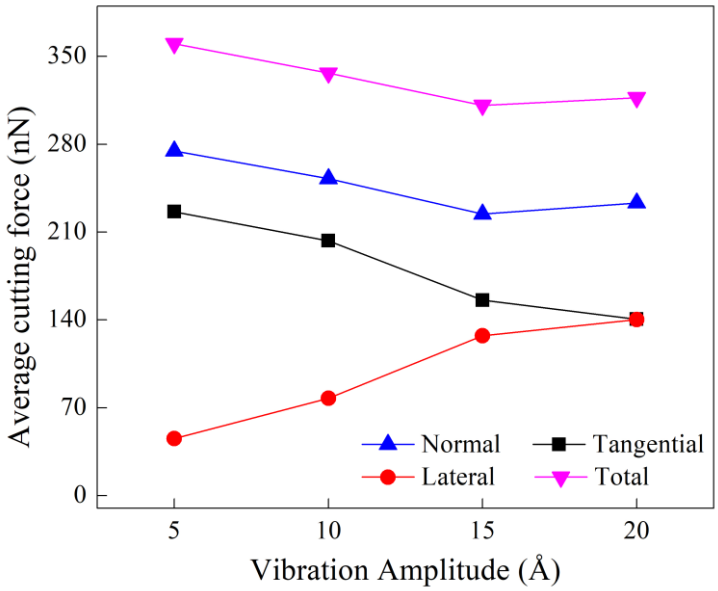


***Figure 8.*** Graph of average cutting force components as a function of vibration amplitude.

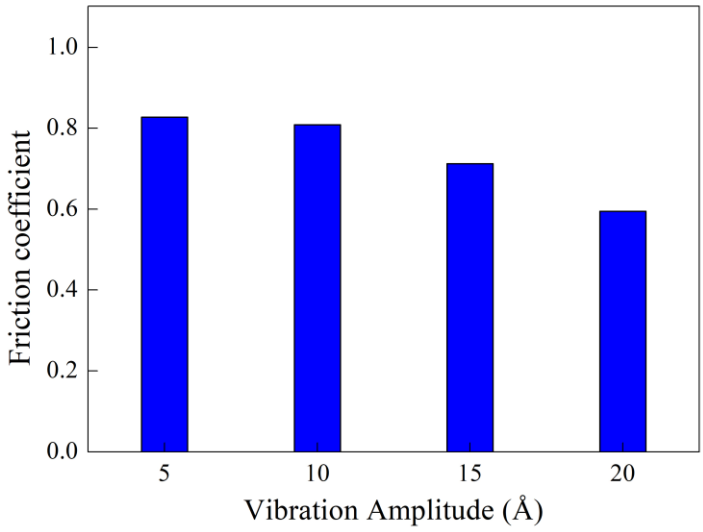


***Figure 9.*** Graph of average friction coefficient as a function of vibration amplitude.

Figure 9 shows the graph of the average friction coefficient as a function of vibration amplitude during steady-state cutting. The result exhibits that the friction coefficient decreases as the vibration amplitude increases. At low amplitudes of 5 Å and 10 Å, the friction coefficient remains around 0.8, indicating that the impact oscillations are not yet sufficient to significantly alter the interaction between the tool and the workpiece. As the amplitude increases to 15 Å and 20 Å, the friction coefficient decreases significantly to below 0.6, suggesting that larger vibrations effectively reduce the actual contact area and contact time between the tool and the surface. Although the trend is not entirely linear, the mechanical and frictional behavior shows that higher vibration amplitudes significantly reduce the average friction coefficient, highlighting the role of intermittent contact created by vibration in promoting more efficient cutting.

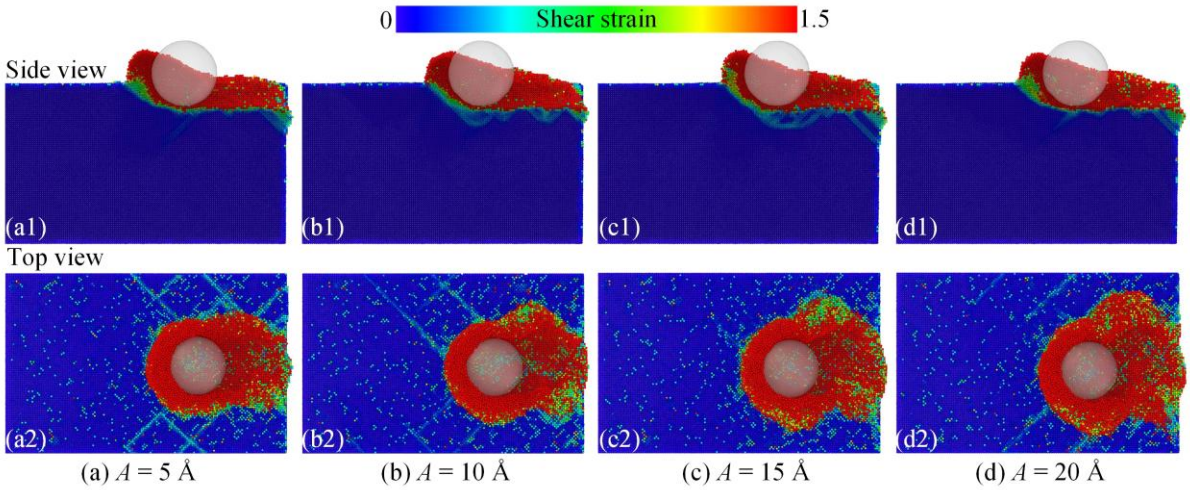


***Figure 10.*** Shear strain distribution in the workpieces after the cutting process with different vibration amplitudes.

Figure 10 shows the shear strain distribution in the workpiece after the cutting process with different vibration amplitudes. At the smallest amplitude $A$ = 5 Å, the plastic deformation zone remains relatively compact, mainly concentrated around the contact area between the tool and the workpiece and along the direction of chip flow. As the amplitude increases to $A$ = 10 Å, both the side view and the top view show a significant expansion of the high deformation zone, indicating enhanced lateral displacement of atoms and more vigorous material flow around the cutting tool. At $A$ = 15 Å, the deformation becomes significantly more pronounced. A larger volume of atoms undergoes high shear strain, especially in the chip and the subsurface region in front of the tool, indicating stronger oscillatory movement that promotes more vigorous plastic cutting and facilitates chip evacuation. At the highest

amplitude $A$ = 20 Å, the high strain zone spreads further in width. This reflects the strong activation of atomic slip events due to the increased vibrational energy, allowing atoms to more easily overcome local energy barriers. Thus, the gradual expansion of the shear strain region with increasing amplitude suggests that ultrasonic vibrations enhance plastic deformation and promote more efficient material removal.

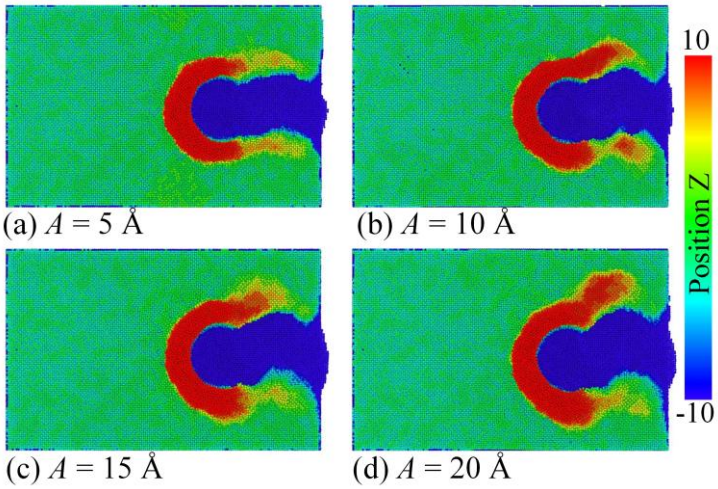


***Figure 11.*** Surface morphology map of workpieces during the cutting process with different vibration amplitudes.

Figure 11 shows the surface morphology during cutting under different vibration amplitudes. The color of the atoms corresponds to the height of the worn atom relative to the original surface height in the Z direction. At an amplitude $A$ = 5 Å, the groove formed behind the tool is relatively narrow, and the lateral material displacement remains limited. The chip accumulation in front of the tool is clearly localized, indicating a stable but narrow material removal process. As the amplitude increases to $A$ = 10 Å, the groove widens, and a large amount of material is pushed up and out, resulting in thicker chips and more pronounced chip piles along both edges of the groove. At $A$ = 15 Å, the deformation becomes more significant, leading to a wider groove and a higher concentration of pushed atoms near the cutting surface. The material flow becomes increasingly dynamic, and the lateral redistribution of worn atoms becomes more apparent. At the highest amplitude $A$ = 20 Å, the oscillating motion causes the widest material displacement. The chip area expands significantly and the chip pile height on both sides increases, reflecting enhanced atomic separation and a greater effective cutting depth. This gradual change suggests that the increased oscillation amplitude promotes stronger interaction between the tool and the surface, accelerating chip formation, and ultimately improving material removal efficiency in VAC. Figure 12 exhibits the number of

worn atoms of workpieces during the cutting process with different vibration amplitudes. The number of abraded atoms increases almost linearly with the cutting distance, indicating continuous atomic separation and chip accumulation during sliding. At the lowest amplitude $A$ = 5 Å, the rate of increase in the number of abraded atoms is smallest due to limited surface penetration and reduced material removal capacity. As the amplitude increases to $A$ = 10 Å and $A$ = 15 Å, the slope of the curve becomes steeper, indicating a higher atom separation rate due to stronger oscillating motion and more positive deformation around the cutting area. At the maximum amplitude $A$ = 20 Å, the number of atom abraded is consistently higher than in other cases across the entire machining distance. This confirms that larger vibration amplitudes significantly increase the separation of surface atoms by increasing the instantaneous distance between the tool and the workpiece, facilitating bond breaking and promoting more efficient chip formation.

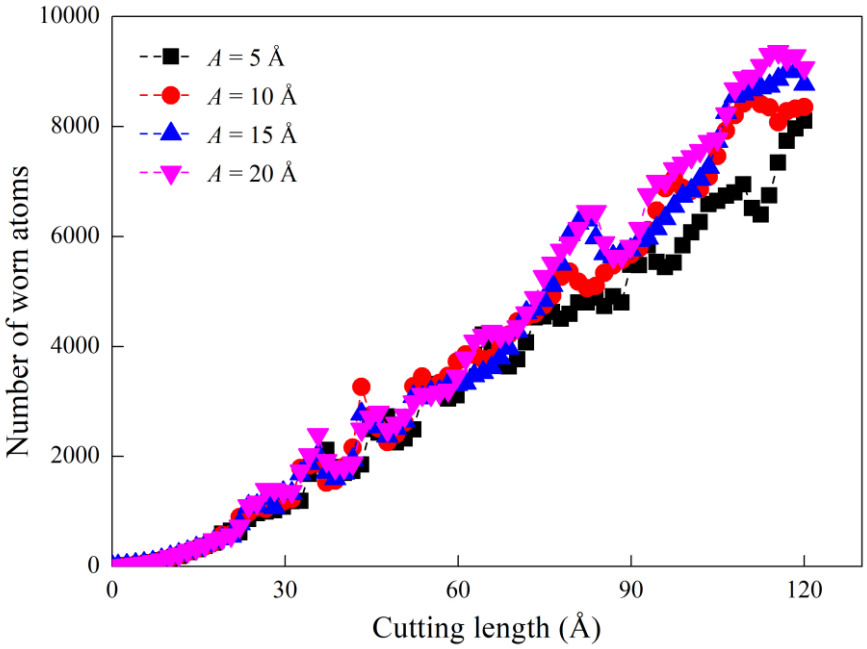


***Figure 12.*** Number of worn atoms of workpieces during the cutting process with different vibration amplitudes.

## 4. Conclusions

In this study, the vibration-assisted cutting (VAC) process of NiCrFe alloy is investigated through molecular dynamics simulation. Its mechanical response and microstructural evolution are systematically compared with conventional cutting (CC) to clarify the effect of vibration amplitude on material removal at the nanoscale. The results show that VAC significantly reduces cutting force and decreases the average friction

coefficient during stable cutting. Microstructural observations reveal that vibration impact promotes interfacial bond disruption and atomic rearrangement, expanding the deformation zone and facilitating more continuous chip formation. The results clearly indicate that VAC provides more efficient and mechanically favorable cutting conditions by weakening the adhesion between the tool and workpiece and enhancing energy transfer at the interface.

The effect of vibration amplitude exhibited a pronounced nonlinear response. Increasing the amplitude leads to a significant reduction in cutting force and friction coefficient, especially beyond 10-15 Å, where periodic contact and separation become more pronounced. Surface morphology and chip characteristics also change strongly with amplitude. At small amplitudes ($A$ = 5 Å), turbulence at the cutting interface is limited, resulting in narrow grooves and moderate material displacement. Conversely, medium and large oscillation amplitudes ($A \geq 10$ Å) produce wider grooves, more chip accumulation, and more worn atoms, due to stronger bond disruption between atoms and an expanded deformation zone. These results demonstrate that vibration amplitude is a crucial parameter governing material removal efficiency. Thus, the VAC process of NiCrFe alloy shows that both mechanical behavior and microstructural evolution are strongly dependent on amplitude, highlighting its importance in optimizing machining performance at the nanoscale.

## References

[1] J. Chen, J. Xiao, L. Zhang, Interdiffusion behaviors between NiCrFe alloy and low-/medium-/high-entropy alloys, *Journal of Alloys and Compounds*, *896* (2022) 162711.

[2] H. Xu, M. Zhang, G. Zhang, G. Li, G. Li, Microstructure and mechanical property of Al, Ti co-adding L21-strengthened NiCrFe-based HEAs, *Materials Characterization*, *207* (2024) 113516.

[3] P. Zhang, X. Zhang, X. Yu, Y. Wang, Research on the nanocutting mechanism of Ni-Fe-Cr-based superalloys: conventional cutting versus UEVC, *Materials Today Communications*, *26* (2021) 101795.

[4] D. Yang, Z. He, M. Zhang, Y. Liu, L. Li, Molecular dynamics investigation of femtosecond laser ablation of Inconel 718 alloy, *Journal of Manufacturing Processes*, *131* (2024) 984-1000.

[5] Y. Fan, S. Yang, Z. Hao, Study on phase transformation in cutting nickel-based superalloy GH4169 based on molecular dynamics, *Journal of Materials Engineering and Performance*, *34* (2025) 11841-11854.

[6] M. Yu, C. Zhang, D. Li, F. Wang, P. Sun, J. Cui, L. Du, Mechanism of surface hardness enhancement of aluminum alloy 2024-T3 by laser-induced plasma electrolyte jet machining, *Surface and Coatings Technology*, *507* (2025) 132141.

[7] F. Ji, Y. An, Y. Xin, H. Guan, Evolutionary trends and research hotspots in electrochemical machining: A bibliometric analysis from 2010 to 2023, *International Journal of Electrochemical Science*, *19* (2024) 100646.

[8] A. Rauf, M.A. Khan, S.H.I. Jaffery, S.I. Butt, Effects of machining parameters, ultrasonic vibrations and cooling conditions on cutting forces and tool wear in meso scale ultrasonic vibrations assisted end-milling (UVAEM) of Ti–6Al–4V under dry, flooded, MQL and cryogenic environments–A statistical analysis, *Journal of Materials Research and Technology*, *30* (2024) 8287-8303.

[9] V. Satpute, D. Huo, J. Hedley, C. Dale, A comprehensive experimental investigation into vibration-assisted micro-milling of monocrystalline silicon, *Journal of Manufacturing Processes*, *131* (2024) 12-26.

[10] C. Zhang, J. Wang, F. Jiao, Y. Cao, Research on tool wear and surface quality in laser-assisted ultrasonic elliptical vibration cutting of cemented carbide, *Tribology International*, *193* (2024) 109389.

[11] R. Jerez-Mesa, Microtexturing of industrial surfaces via radial ultrasonic vibration-assisted machining: An analytical model and experimental validation, *Surface and Coatings Technology*, *482* (2024) 130718.

[12] D.-Q. Doan, T.-H. Fang, Effect of vibration parameters on the material removal characteristics of high-entropy alloy in scratching, *International Journal of Mechanical Sciences*, *232* (2022) 107597.

[13] A. Shamsi, M.S. Khan, D.K. Yadav, M. Shahwan, M. Furkan, R.H. Khan, Structure-based drug-development study against fibroblast growth factor receptor 2: molecular docking and Molecular dynamics simulation approaches, *Scientific Reports*, *14* (2024) 19439.

[14] Z. Ren, R. Feng, B. Zhou, H. Cao, H. Li, W. Yang, C. Lei, Molecular dynamics simulation for temperature assisted machining of a polycrystalline γ-TiAl alloy, *Journal of Manufacturing Processes*, *132* (2024) 615-628.

[15] A.B.M. Ali, D.J. Jasim, A.a. Alizadeh, C.K. Chan, S. Salahshour, M. Hekmatifar, A molecular dynamics study of the effect of initial pressure on the mechanical resilience of aluminum polycrystalline, *Results in Engineering*, *24* (2024) 102879.

[16] T.-X. Bui, T.-H. Fang, C.-I. Lee, Effects of inclusion type and inclusion radius on deformation characteristic and failure mechanism inside monocrystalline NiFeCr alloy, *Journal of Alloys and Compounds*, *962* (2023) 171062.

[17] X.-Y. Song, X.-B. Liu, A. Zhou, F.-Z. Zhang, Z.-Y. Liu, J. Xia, S.-H. Zhang, Effect of mixing entropy on nano-scratching behavior in FCC polycrystalline MPEAs: A comprehensive study by molecular dynamics simulation and experiment integration, *Tribology International*, *200* (2024) 110088.

[18] A.P. Thompson, H.M. Aktulga, R. Berger, D.S. Bolintineanu, W.M. Brown, P.S. Crozier, P.J. In't Veld, A. Kohlmeyer, S.G. Moore, T.D. Nguyen, LAMMPS-a flexible simulation tool for particle-based materials modeling at the atomic, meso, and continuum scales, *Computer physics communications*, *271* (2022) 108171.

[19] A. Stukowski, Visualization and analysis of atomistic simulation data with OVITO–the Open Visualization Tool, *Modelling and simulation in materials science and engineering*, *18* (2009) 015012.